Journal of the European Ceramic Society 22 (2002) 2697–2707

www.elsevier.com/locate/jeurceramsoc

Effect of microstructure on the fracture behavior of biomorphous silicon carbide ceramics

Peter Greil[a,*], Evelina Vogli[a], Tobias Fey[a], Alexander Bezold[a], Nadja Popovska[b], Helmut Gerhard[a], Heino Sieber[a]

[a]*Department of Materials Science (Glass and Ceramics), University of Erlangen-Nuernberg, Martensstr. 5, D-91058 Erlangen, Germany*
[b]*Department of Chemical Engineering, University of Erlangen-Nuernberg, Egerlandstr. 3, D-91058 Erlangen, Germany*

Received 7 October 2001; received in revised form 22 February 2002; accepted 8 March 2002

Abstract

Highly porous cellular silicon carbide was prepared from native pine wood tissue by vapor infiltration of Si, SiO, and CH_3SiCl_3 into the carbonized template. β-SiC at the biocarbon surface finally resulted in a complete conversion of the template into a cellular silicon carbide material. Due to the different reaction mechanisms, different strut microstructures were obtained. The strength of the biomorphous SiC was measured under biaxial tensile loading conditions perpendicular to the cell elongation (in-plane loading). A non-catastrophic stress-strain behavior was observed in the Si and CH_3SiCl_3 derived materials which showed a high skeleton density of $\geqslant 3$ g/cm^3. Extendend cell wall fracture (peeling) was observed in the Si derived material where the original intercellular lamella was retained in the ceramic material. FE calculations of the stress distribution in a representative structure model showed significantly lower levels of tensile stress in rectangular pore arrays (early wood tissue) compared to ellipsoidal pores (late wood tissue).

Keywords: Biomorphous SiC ceramics; Microstructure and strength

1. Introduction

Woods are cellular solids, composed of mixed biopolymers (cellulose fibers, lignin and hemicellulose as matrix material), and with a relative density ranging from less than 0.05 to almost 1. Extended structure analyses of wood using micro-beam scanning X-ray scattering revealed a microstructure with highly oriented cellulose fibers at the nanometer level of the cell wall,[1] which is supposed to be responsible for the unique mechanical stability (elasticity, strength and toughness) of living trees under harsh mechanical loading conditions. The highly anisotropic cellular structure of wood tissue may serve as a hierarchically structured template to generate novel cellular ceramics with micro-, meso-, and macro-structures pseudomorphous to the initial porous tissue skeleton spanning in typical dimensions from nanometers (cellulose microfibrils) to the centimeter level (wood tissue).[2] The inherent vascular transportation system of wood which consists of large pore channels (vessels) with a diameter of 30–45 μm in soft woods and 10–400 μm in hard woods provides rapid access for gaseous or liquid infiltrants which may be used for ceramic conversion.

Cellular silicon carbide ceramics have recently been prepared from native wood structures (for review see Ref. 3). Basic approaches for materials manufacturing using cellulose precursor structures (often called *CDC* process, Cellulose Derived Composites) generally include three steps: carbonization, shaping, and conversion to final material.[3,4] The unique anatomical features of the native plant tissue can be retained during pyrolysis in inert atmosphere, which yields a porous template composed primarily of the element carbon.[5] Instead of native wood tissue, wood fiber materials such as medium density fiber (MDF) boards can also be used as the base material with an improved homogeneity compared to the highly heterogeneous grown materials.[6]

* Corresponding author. Tel.: +49-9131-852-7543; fax: +49-9131-852-8311.
E-mail address: greil@ww.uni-erlangen.de (P. Greil).

0955-2219/02/$ - see front matter
PII: S0955-2219(02)00135-8

After pyrolysis, the shaped biocarbon template can subsequently be infiltrated with gaseous or liquid silicon bearing precursors such as silicon melt, silicon and silicon monoxide vapor, or organosilicon compounds.[3,7–11] During infiltration the Si-precursors react at the carbon surface to form cellular silicon carbide mainly consisting of β-SiC. The phase formation and microstructure evolution depends on the reaction conditions as well as residual amounts of free silicon or free carbon.

While the mechanical properties of native wood have been a matter of extended investigation,[12,13] less results have yet been published on the mechanical behavior of ceramics manufactured from wood (often called "*ceramic wood*"). Generally, the mechanical properties (strength, elastic modulus, toughness) of wood derived ceramics increase with fractional density. A fracture strength of >330 MPa, an approximate fracture toughness of 3 MPa$\sqrt{m}$ and a Young's modulus of 300 GPa were reported for biomorphous SiSiC with a density of 2.8 g/cm^3.[9] Good high temperature strength was found up to 1350 °C which was attributed to the formation of an interconnected network of SiC.[14] Strength and strain-to-failure of liquid Si infiltrated biomorphous SiSiC materials pseudomorphous to a variety of soft (balsa, pine) and hard woods (maple, oak, beech, ebony) were found to exhibit significantly higher values in axial loading direction i.e. parallel to the cell elongation, compared to loading in radial and tangential directions.[8] It was found, that compared to conventionally fabricated SiSiC of the same overall phase composition but isotropic pore distribution, the biomorphous SiSiC ceramics attained a higher strength (in axial direction) at the same level of porosity. A waved and graduated fracture path was observed, which was associated with undulations of low and high density regions (according to the growth ring patterns) giving rise for a variation of the crack resistance in the crack extension direction and non-linear stress–strain curves.[15]

The study of mechanical properties of biomorphous materials consists in developing the connections within and between the various representative volume elements. Due to the hierarchical structure of biological tissue, the representative volume element over which the average of mechanical properties are representative of the whole can be quite large (10^3 mm^3) compared to conventional engineering materials (down to 10^{-12} mm^3).[2] Generally, averaging techniques from solid mechanics theories (rule of mixtures for composites, laminate theories) are used, which, however, is associated with the loss of some information of the subsystem in the process. This is particularly relevant in relation to mechanical events occurring at local levels, such as damage initiation and fracture propagation, for example, as opposed to global events such as elastic behavior or structural instabilities of the kind associated with buckling and fracture.

It is the aim of this work to examine the fracture behavior of low density biomorphous SiC ceramics. Low density β-SiC ceramics (fractional density 0.2–0.3) were prepared from a soft wood (pine) which has no large vessels and hence a more homogeneous cellular structure compared to hard woods. In order to modify the strut density and microstructure three different gaseous Si-precursor systems (Si, SiO, CH_3SiCl_3) were used for infiltration of the porous biocarbon template. Biaxial tensile loading perpendicular to the axial direction was applied and the fracture behavior was analyzed. FE calculations of the stress distribution in the ceramic struts between the pores suggest that cell geometry and cell arrangement might have an impact on the local fracture processes.

2. Experimental procedure

2.1. Manufacturing of biomorphous silicon carbide

Samples were prepared from coniferous pine wood (*Pinus silvestris* L.). Pine was chosen because of its relatively homogeneous tracheidal pore structure with a mean trachedial pore channel diameter of 20 μm. It exhibits an uniform morphology of 90–95 vol.% Tracheids, which serve for the axial (parallel to the stem) water conduction and mechanical support in the living tree. The tracheids are typically 1–5 mm in length and the cell walls contain a large number of pits.

A vapor phase infiltration technique was applied to manufacture biomorphous SiC from biocarbon templates. Monoliths of dried wood (70 °C for 24 h) were heated in inert atmosphere with a slow heating rate of 1 °C/min up to 500 °C to avoid crack formation[5] and 5 °C/min up to a peak temperature of 800 °C. The specimens were hold for 4 h to allow rearrangement of the polyaromatic carbon structures. During pyrolysis, H_2O, CO_2 and CO were released as the major volatile species giving rise for a weight loss of 68 wt.% and a linear shrinkage of 22% (axial e.g. parallel to stem axis) to 28% (radial e.g. perpendicular to stem axis).

Different SiC microstructures were obtained by using three different vapor sources: Si, SiO and CH_3SiCl_3. While in the case of Si and SiO the infiltration and reaction temperature is high (1600 °C), both vapor transport and interface carbide reaction are concurrent processes. In contrast infiltration of CH_3SiCl_3 operated at 850 °C followed by a high temperature annealing step at 1600 °C. Monoliths of the biocarbon template with sizes of $20\times20\times2$ mm^3 were placed in a glassy-carbon crucible in an Al_2O_3 tube. Heat treatment in Ar-atmosphere at 1600 °C for 8 h caused the Si-precursor to diffuse into the porous biocarbon template. Si vapor was produced by melting Si powder in a carbon crucible below the specimen and SiO was obtained from an

equimolar mixture of Si and SiO_2 powder.[11] At 1600 °C the effective partial pressures of Si and SiO attained 10^{-5} and 10^{-3} MPa, respectively, which are high enough to achieve complete infiltration and reaction within reasonable cycle times.

A mixture of gaseous CH_3SiCl_3 and H_2 using He as the transport gas was injected into a quartz tube reactor operated at 850 °C. The CH_3SiCl_3/H_2 ratio was varied between 1:(8–12) in order to adjust reasonable reaction conditions for deposition of Si and Si + SiC rather than C in the porous template.[16] A first annealing step at 1200 °C for 1 h was followed by a second heating to 1600 °C. Si melted and reacted with the carbon of the original cell walls to form β-SiC. Thus, the strut microstructure was characterized by a core layer of reaction formed SiC covered on both sides by a 1–2 μm thick layer of CVD-SiC.

2.2. Microstructure characterization

The bulk density (geometrical density) was determined by measuring the weight and the volume of the cylindrical specimens. The skeleton density (strut density) was derived from He-pycnometry measurements (Accupyc 1330, Micromeretics, Norcross, GA). The specific surface area was determined by N_2 adsorption method according to the BET method (ASAP 2000, Micromeretics, Norcross, GA). The mean strut thickness was estimated by direct measurement of the struts in axial cuts from SEM micrographs.

2.3. Strength measurements

The strength of the biomorphous ceramics was measured using a biaxial flexure test where the specimen rests on a ring and load is applied at center with a ball (ball-on-ring), Fig. 1. Central loading was applied in the longitudinal direction (X_3) resulting in an *in-plane* biaxial tensile stress state (X_1, X_2) at the bottom of the cylindrical sample surface. Tensile loading in the radial and tangential directions is more sensitive to the cell microstructure e.g. geometry, size, and packing arrangement, compared to the "strong" longitudinal cell elongation direction. Generally, theoretical considerations predict that the *in-plane* strength, in every instance, is lower than that for *out-of-plane* loading because bending of the cell walls dominates in the first case, axial deformation in the second direction.[12]

Disc-like specimens were prepared from the biomorphous ceramic materials by cutting slices with a thickness of 1–3 mm and a diameter of 25–30 mm. The discs were tested as prepared, no polishing was applied. A steel ball with a diameter of 2 mm was used for central loading the disc specimen on a support steel ring with a diameter of 18 mm. A high loading rate (cross head velocity) of 1 mm/min was applied to obtain the

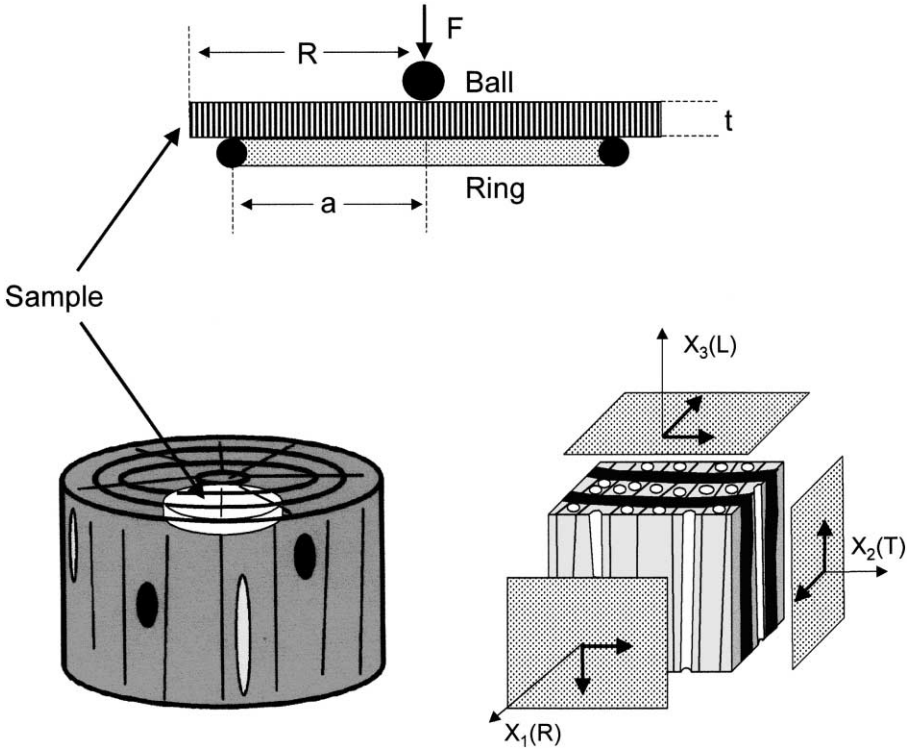

Fig. 1. Conditions of the mechanical testing procedure: ball-on-ring test geometry (top), sample orientation (bottom left) and loading orientation (bottom right).

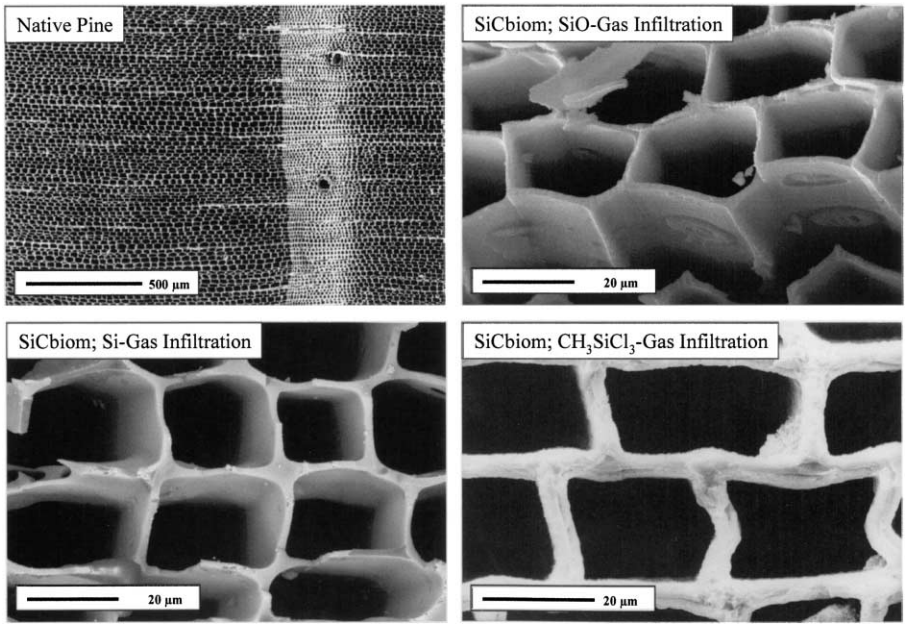

Fig. 2. SEM micrographs of the cellular microstructures of the native tissue of pine (*Pinus silvestris*) and the biomorphous SiC ceramics.

strength which corresponds to the inert value (assuming that no slow crack growth took place). The tensile fracture stress, σ_{max}, was obtained from the relation.[17]

$$\sigma_{max} = \frac{3F(1+\upsilon)}{4\pi t^2}\left[1+2\ln\left(\frac{a}{b}\right)+\frac{(1-\upsilon)}{(1+\upsilon)}\left\{1-\frac{b^2}{2a^2}\right\}\frac{a^2}{R^2}\right] \quad (1)$$

where F is the load at fracture, υ the Poisson's ratio (0.15 for SiC), t the specimen thickness and R the specimen radius, a the radius of support ring (18 mm) and b the radius of region of uniform loading at center ($b \approx t/3$). The strain, ϵ, was derived by measurement of the central deflection, s, using the following expression: $\varepsilon = (ts)/a^2$.

2.4. FE calculations

The finite element method was selected as a vehicle for modeling the stress distribution of representative volume segments subjected under transverse (perpendicular to the axial direction) tensile loading. A 3D mesh of a regular array of quadratic and ellipsoidal pores was generated using FE software packages.[18] A total number of up to 400 000 three dimensional 20 node brick elements were applied in the calculations. As boundary conditions an uniaxial tensile stress of 10 MPa was applied to the surface and nodal displacements were fixed except for the loaded surface. The material parameters of β-SiC were taken into account for the calculations (Young's modulus 410 GPa, Poisson ratio 0.15, Density (ρ_s) 3.1 g/cm^3, Weibull-modulus 8).

Table 1
Microstructural characterization of SiC_{biom} pseudomorphous to pine

	Wood	Biocarbon template	Silicon carbide		
			SiO	Si	CH_3SiCl_3
Density (g/cm^3)					
Geometrical	0.47	0.34	0.6	1.0	1.2
Skeleton	1.4	1.4	2.5[a]	3.1	3.1
Porosity (%)	67	76	80	70	60
Specific surface area (m^2/g)	–	46	16.1	3.3	0.5
Mean strut thickness[b] (µm)	2	1.5	1	2	4

[a] Skeleton density increased upon annealing to 1600 °C due to sintering.
[b] Early wood cells.

3. Results and discussion

3.1. Microstructure of biomorphous SiC

Fig. 2 shows the cellular microstructures (axial sections) of the biomorphous SiC-materials obtained from different Si-containing vapor precursors. The cellular tissue of native pine consists of regular tracheidal cells, most of them show a square or rectangular shape. The uniform cell arrangement of early wood is interrupted by growth ring patterns, where late wood cells show a significantly higher strut thickness and hence a reduced cell diamter. A few large resin canals are present. Generally, the biomorphous SiC_{biom} forms an interconnected network reproducing the original cellular anatomy of the wood tissue. The SiO-infiltrated material shows a higher porosity of 80% compared to 70% of the Si-vapor and 60% of the CH_3SiCl_3 derived ceramics. Table 1 summarizes the characteristic microstructural features of the various silicon carbide materials prepared from pine.

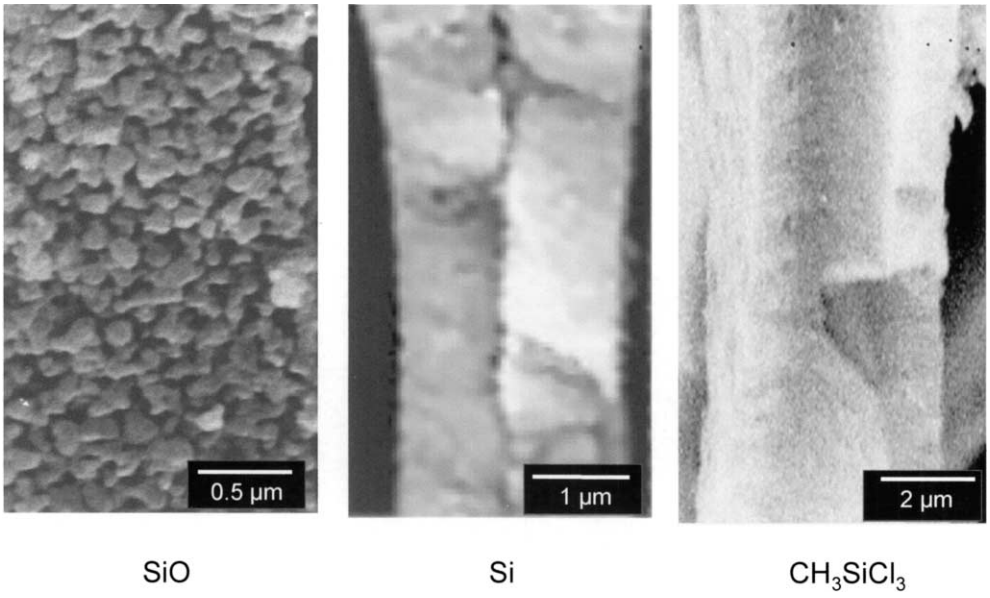

Fig. 3. SEM micrographs of the different strut microstructures resulting from different silicon containing gas phase precursors.

Fig. 3 shows the strut microstuctures of the three materials. Significant differences of the original cell wall structure (struts) are related to the different precursor phases and reaction mechanisms. The SiO derived material shows a uniform microstructure of submicron β-SiC (mean particle size <0.4 μm) with a pronounced porosity of approximately 80%. Half of the initial carbon is supposed to be released from the template via CO(g) evaporation leaving a substationally higher porosity in the cell wall:[19]

$$2C(s) + SiO(g) \rightarrow SiC(s) + CO(g) \quad (2a)$$

From SEM observations it was concluded that the SiC forming the cell wall material between the cells is highly porous only in the initial state of reaction, making rapid gas phase transport possible. After prolonged annealing at 1600 °C, however, sintering may occur when the particle sizes are in the submicron range, resulting in a densification of the strut material and a low mean strut thickness (early wood tissue) of 1 μm.[11]

In contrast, the Si derived ceramic is characterized by a dense strut material:

$$C(s) + Si(g) \rightarrow SiC(s) \quad (2b)$$

Once a continous SiC reaction layer has formed at the biocarbon surface, solid state diffusion of Si and C via grain boundaries is supposed to control further silicon carbide film growth.[3] Analyses of multilayer growth experiments suggested that the reaction proceeds at the SiC–C interface, which is possible only when the Si diffuses through the SiC layer.[19] The constrained growth may result in an elongated SiC particle morphology with the growth direction perpendicular to the surface. The original intercellular lamella is supposed to act as a growth barrier and the original lamella separating the cells can clearly be seen in the silicon carbide material, Fig. 3b. The strut thickness is approximately 2 μm which is almost the same as in the biocarbon template.

Infiltration of CH_3SiCl_3/H_2 into the biocarbon template at 850 °C resulted in the deposition of SiC and Si which can be expressed by a simplified chemical vapor deposition reaction

$$2\ CH_3SiCl_3(g) + 2\ H_2(g) \rightarrow Si(s) + SiC(s) + 6\ HCl(g) + CH_4(g) \quad (2c)$$

Subsequent heating above the melting temperature of Si (1410 °C) gives rise for a liquid infiltration process which is localized to the cell wall area. The molten Si can wet and penetrate into the carbon struts and react to form β-SiC. A typical multilayer strut microstructure is formed with an inner core of dense (liquid infiltration) SiC and an outer layer of porous (chemical vapor deposition) SiC. Due to the deposition of SiC a significantly larger mean strut thickness of 4 μm was observed.

3.2. Fracture behavior

As the original wood anatomy is highly anisotropic, the propagation of cracks in the biomorphous ceramic will depend on, among other factors, the direction in which the crack grows. In native wood six different systems of crack propagation (longitudinal, radial, tangential and the equivalent directions) where addressed.[20]

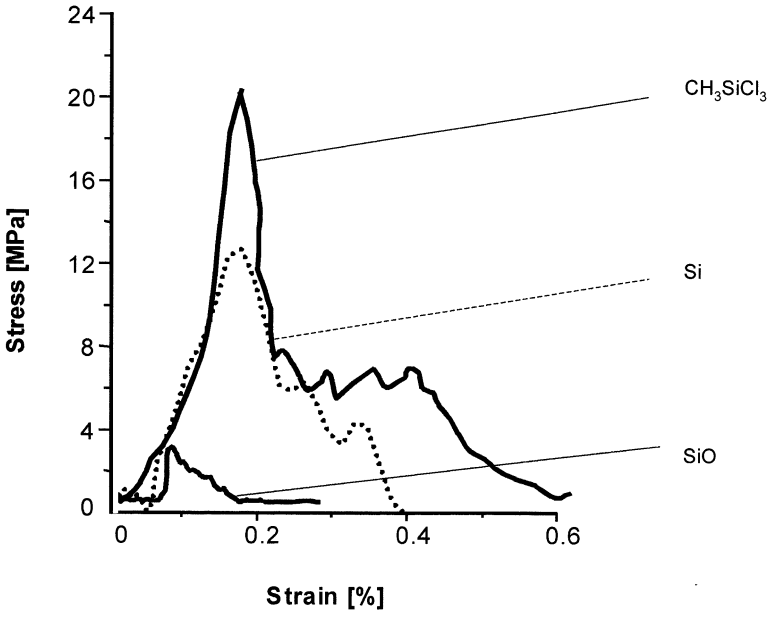

Fig. 4. Stress vs. strain diagrams of the gas phase synthesized biomorphous SiC under biaxial (X_1, X_2) tensile loading conditions.

(Fig. 1). Brittle cellular ceramics of high porosity fail abruptly at a stress which is usually lower than the strength of the bulk material. In compression the cells suffer progressive crushing, in tension the cellular structure fails by fast brittle fracture. As with any brittle solid, fracture in tension is controlled by the largest defect (a crack, or notch, or cluster of damaged cells).

Fig. 4 shows the stress-strain diagrams for the specimens biaxially loaded in the *ball-on-ring* test. The facture stress strongly increased from approximately 4 Mpa (SiO) to 13 MPa (Si) and 21 MPa (CH_3SiCl_3) at fractional densities increasing from 0.2 to 0.3 and 0.4, respectively. All specimens exhibit a non-catastrophic failure behavior with a maximum failure strain of 0.6% (CH_3SiCl_3). Each stress drop is associated with fracture of several layers of cells. The area under the stress–strain curve is related to the energy dissipated by the sample during non-catastrophic fracture.

From the analyses of failure mechanisms occuring in fibrous monolithic ceramics which have a structure very similar to that of wood derived ceramics, tensile failure by cell fracture as well as cell wall fracture and shear failure are supposed to dominate the micromechanical fracture processes.[21] The fracture process that occurrs in these materials was described by existing theories for the fracture of two-dimensional layered materials after modification to account for the unique structure of fibrous monoliths. Tensile failure by cell fracture was supposed to dominate when the cell boundaries are tough in comparison to that of the cells. Cell wall failure is likely to occur when the cell boundaries are weak compared to the cells.

Fig. 5a and b shows the fracture surfaces of the Si-gas infiltrated silicon carbide. Microstructural features of a non-colinear crack propagation similar to crack kinking patterns in multilayer composites can be observed. Thus, Fig. 5a shows an area of the fracture surface which is oriented perpendicular to the longitudinal (X_3) direction. Microscopic examination shows evidence for a pronounced *cell-wall-peeling* type of crack propagation which is confirmed by the tangential plane orientation presented in Fig. 5b. Similar features of cell wall peeling were observed in the CH_3SiCl_3-derived material which showed similar intercellular lamella structures as in the Si-derived material. In contrast, no indication of interface controlled crack growth could be found in the SiO-infiltrated SiC_{biom} material.

Local failure of a single cell does not necessarily cause global failure when load can be transferred to the neighboring cells. This behavior is favored when there are many cells in the specimen and variability in the strength of the cells is high.[22] Because the failure of fibrous monoliths is controlled by damage accumulation, the strength should be less sensitive to preexisting flaws than either monlithic ceramics or simple laminates.

3.3. Influence of material properties

The specimens failed under a biaxial state of tensile stress when the maximum principal stress reached a critical value σ_c. Following Gibson and Ashby[12] the relative strength for elastic collapse of cellular structures (σ_c/σ_s, where σ_c is the strength of the cellular structure and σ_s the strength of the fully dense material) can be related with the relative density (ρ_c/ρ_s, where ρ_c is the

density of the cellular structure and ρ_s the density of the fully dense material) by:

$$\textit{out-of-plane}\ (X_3): \left.\frac{\sigma_c}{\sigma_s}\right|_{X_3} = C_1 \frac{\rho_c}{\rho_s} \tag{3a}$$

$$\textit{in-plane}\ (X_1,\ X_2): \left.\frac{\sigma_c}{\sigma_s}\right|_{X_{1,2}} = C_2 \left(\frac{\rho_c}{\rho_s}\right)^2 \tag{3b}$$

C_i is a numerical constant depending on the geometric characteristics of the cell structure e.g. square or hexagonal cell anatomy. The scaling parameter n_i takes into account the loading directions with respect to the cell orientation and the deformation mode of the struts [$n=1$ in axial (*out-of-plane*) and $n=2$ in radial and tangential directions (*in-plane*)]. Assuming reasonable values for the strut strength σ_s and the strut density ρ_s in the order of 400–600 MPa (bending) and 3.2 g/cm^3 for

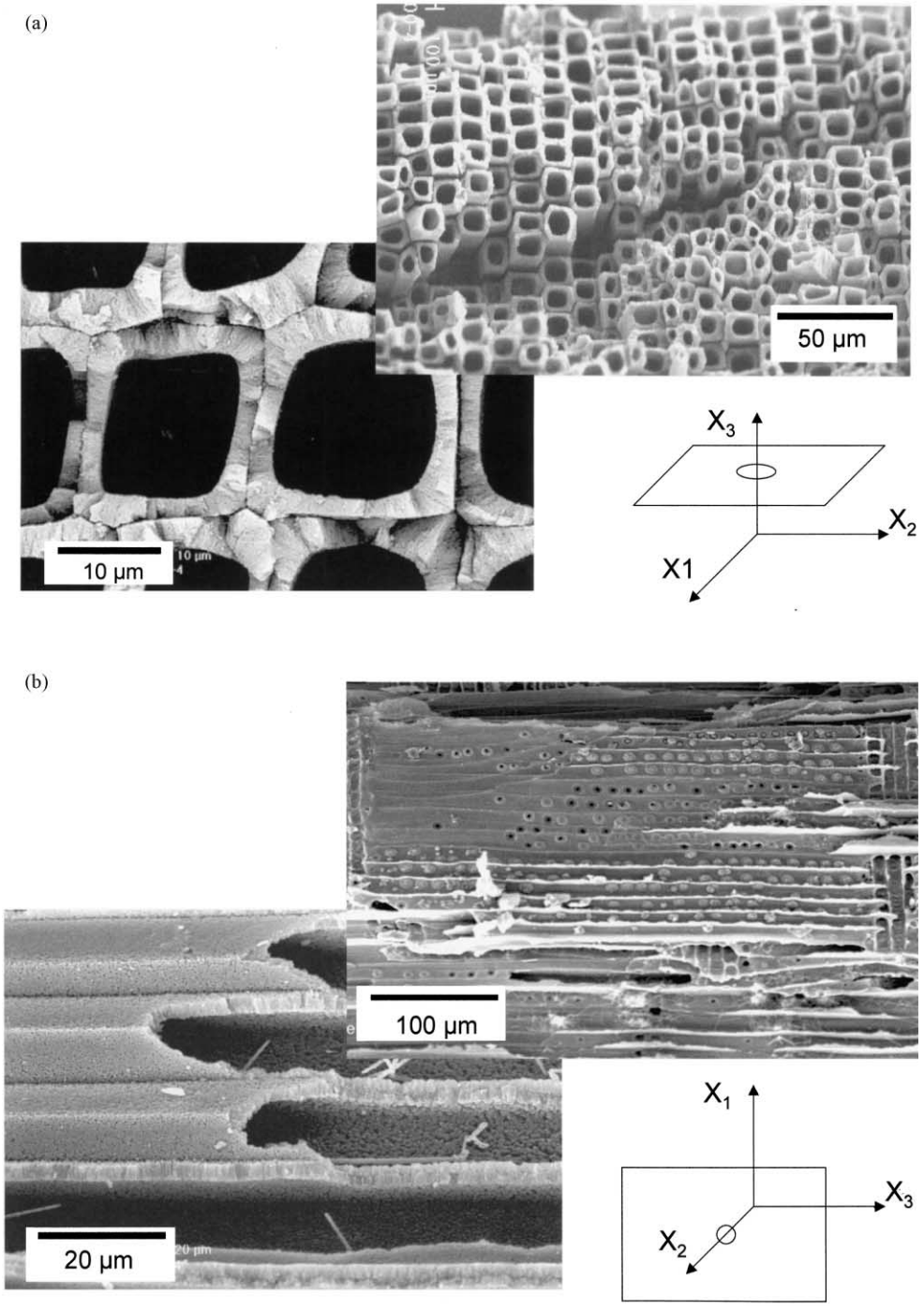

Fig. 5. Fracture surface of Si-vapor infiltrated SiC: (a) fracture surface orientation (001) i.e. perpendicular to the axial cell elongation direction and (b) fracture surface (010) i.e. parallel to the axial cell orientation (tangential plane).

dense SiC and 90–130 MPa and 2.24 g/cm^3 for SiC with a porosity of 30% (calculated from $\sigma_p = \sigma_0 \exp(-5V_p)$ with $\sigma_0 = 400$–600 MPa and $V_p = 0.3$) an estimated value of $C_2 \cong 0.20$–0.35 was derived from the experimental data. These values are slightly higher as found for regular honeycomb structures where C_2 varied from 0.14 in the tangential to 0.2 in the radial direction (with $C_1 = 0.34$ in the axial direction).[12]

Increasing the fractional density, ρ_c/ρ_s, as well as otimizing the fracture strength of the strut material, σ_s, are the primary strategies to improve fracture resistance of highly porous cellular ceramics. For a low density regular honeycomb with square cell morphology, which in a first approximation may serve as a reasonable model for the cell anatomy in pine wood (Fig. 2), fractional density can be expressed in terms of the strut thickness t and the cell length l by:[12]

$$\frac{\rho_c}{\rho_s} = 2\frac{t}{l}\left(1 - \frac{t}{2l}\right), \tag{4}$$

so that the fracture strength of the cellular ceramic, σ_c, scales with $(t/l)^n$. While the cell size, l, is given by the growth anatomy of the native plant, strut thickness t may be controlled by appropriate processing techniques as demonstrated in this work.

Fracture strength optimization of the strut material, σ_s, involves minimization of flaws and porosity within the struts and maximise toughness (fracture mechanics approach). An increase in strut strength would be expected as a result of the reduced probability of finding a critical flaw in a smaller volume of material as predicted by a Weibull weakest link hypothesis for strength variability. As the cell size decreases, the strut volume, as well as the strut surface area decrease. Alternatively, processing differences to produce materials with differing cell sizes and densities could influence σ_s. Thus, for a strut material with a Weibull modulus m, the effect of cell size was described with a relation of the type:[12]

$$\frac{\sigma_{s,1}}{\sigma_{s,1}} = \left(\frac{l_2}{l_1}\right)^{2/m}\left(\frac{\rho_{c,2}}{\rho_{c,1}}\right)^{1/m}. \tag{5}$$

Accordingly, the ratio of fracture toughnesses of two specimens of cellular ceramics of equal total volume and identical cell shape but with different cell sizes is:

$$\frac{K_{Ic,1}}{K_{Ic,2}} = \left(\frac{l_1}{l_2}\right)^{\frac{1}{2}-\frac{2}{m}}\left[\frac{\rho_{c,1}}{\rho_{c,2}}\right]^{2-\frac{1}{m}}. \tag{6}$$

Local variation of fracture toughness is expected to occur when when the cell size, strut thickness, and cell morphology are changed. For loading directions parallel to the tracheidal pore system, for example, undulations of low and high density regions (growth ring patterns and rays) are likely to affect crack propagation in the crack extension direction. Evaluation of the ceramic microstructures indicates a reduction of cell size l by a factor of 3 and an increase of strut thickness t by a factor of 3 at the early wood to late wood transition. Thus, for a reasonable

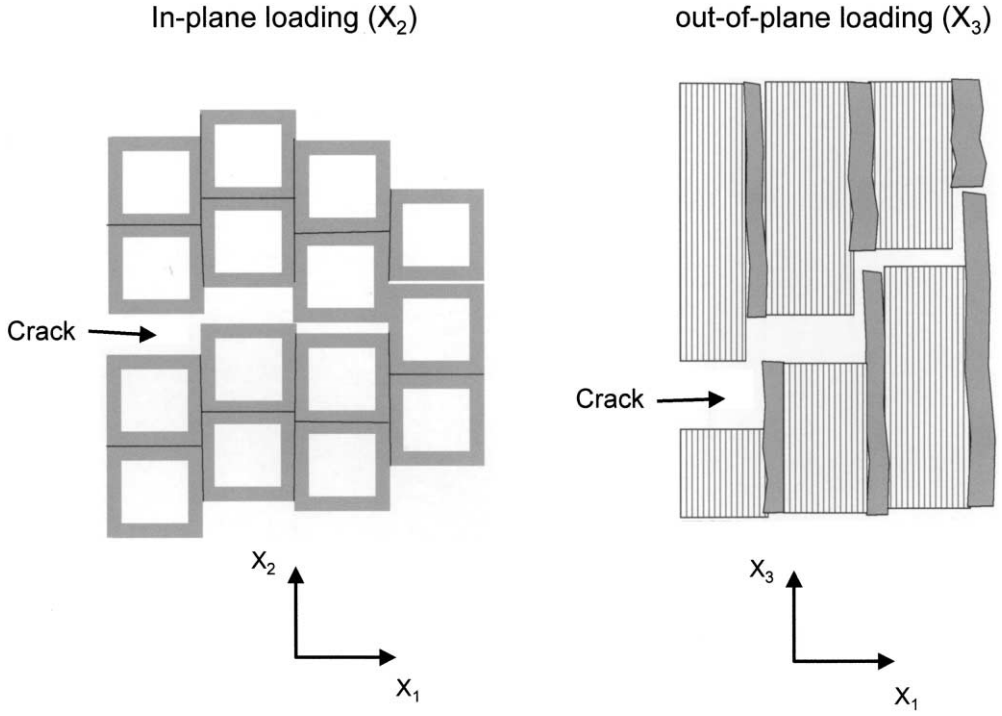

Fig. 6. Schematic model of the crack propagation path for different loading orientation: in-plane loading with tensile stress in X_2 direction (left) and out-of plane loading with tensile stress in X_3 directon (right).

Weibull modulus of SiC of 8 an increase of fracture toughness by 30% and of strength by 25% is estimated. Thus, the transition regions might act as crack deflecting interfaces[23] with the layers cracking sequentially giving a series of steplike drops in the stress-strain response following the onset of cracking.[24] Fig. 6 shows a schematic of the micromechanical crack processes which may occur depending on the loading conditions applied.

3.4. FE-calculations of stress distribution in the cell walls

The local stress distribution in the cell walls of a volume segment representing the characteristic structural features of the SiC_{biom} ceramic was calculated using a three dimensioal FE model. A uniaxial remote stress of 10 MPa acting in X_1 direction i.e. perpendicular to the cell elongation direction was applied. Fig. 7 shows the distribution of the normal stress component parallel to the applied stress for cell morphology transition area where a square cell geometry dominates in the early wood area and an ellipsoidal cell geometry in the late wood area. Strut thickness and cell size and shape parameters where taken from experimental data.

As may be seen, square cells loaded in transverse direction exhibit a significantly lower tensile stresses at the same level of fractional density compared to spherical pores. At a porosity of 65% the maximum tensile

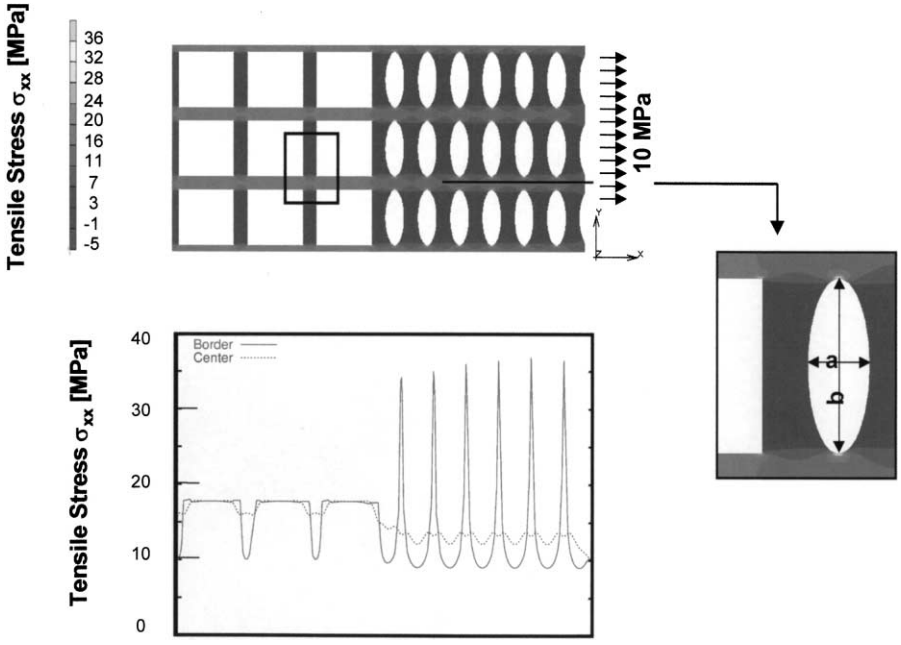

Fig. 7. Distribution of the normal stress component, σ_{xx}, parallel to the applied tensile stress for the cell morphology transition area (left: early wood, right: late wood anatomy) calculated by FEM.

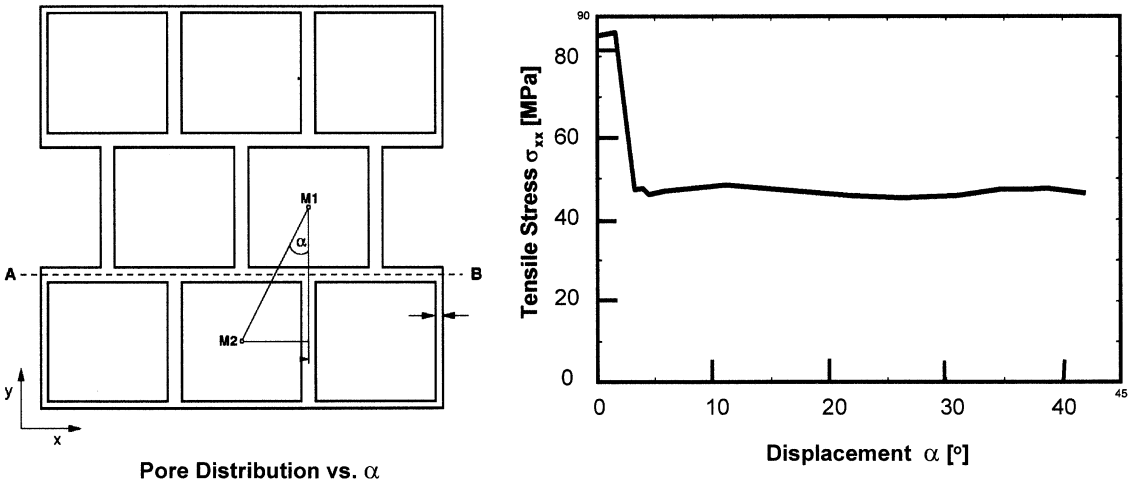

Fig. 8. Effect of cell packing structure on the maximum tensile stress in the strut (same loading orientation as in Fig. 7).

stress between the nodes in the square cell pattern is less than 20 MPa whereas tensile stresses exceeding 35 MPa were obtained at the sharp edges of the ellipsoidal cells. Despite the significantly higher fractional density and strut thickness the area at the transition from early to late wood tissue anatomy may give rise for increased probability of crack formation under the loading conditions considered.

The effect of cell packing structure on tensile stress distribution is given in Fig. 8. A regular square type of cell pattern is packed either with a shift angle $\alpha = 0$ e.g. a four node fitting, and a three node structure when $\alpha > 0$. An abrupt reduction of the tensile stress from 80 MPa down to less than 45 MPa is found even at small deviations when $\alpha > 2$–3°. Thus, transversly loaded cell packing structures may show distinct differences in loading stresses depending on the local packing structure and loading direction. Crack advance is likely to be localized on the highly stressed areas whereas optimum packing should yield higher fracture resistant segments in the loaded structure.

4. Conclusions

Biomorphous silicon carbide ceramics with a cellular micro- and macrostructure pseudomorphous no naturally grown wood tissue show a complex mechanical behavior which is goverend by the unique arrangement of cells. In some aspects, the fracture behavior in biomorphous ceramics is similar to that of fibrous monolithic ceramics as well as that of laminate composite ceramics showing a non-catastrophic stress–strain behavior. A pronounced anisotropy of fracture behavior is a characteristic feature which depends on the loading conditions with respect to the orientation of the cell packing structure.

Fracture of the cell wall as well as of the cell interface (intercellular lamella) is supposed to dominate the micromechanical crack propagation. The energy absorption capacitiy of biomorphous ceramics is supposed to be governed by cracking and frictional sliding. Both of these mechanisms are more effective when extensive delamination occurs prior to the fracture of the individual cells [Ref. 21]. Thus, tailoring of the strut microstructure and the interface bewteen the cells by suitable processing techniques seems to play a key role for improving the mechanical properties of low density biomorphous silicon carbide ceramics. It was shown, that increasing the cell wall (strut) thickness and density resulted in an improvement of fracture strength of the highly porous (porosity 60–80%) material.

Highly porous cellular silicon carbide materials may be of interest as high temperature resistant catalyst and filter support structures. The directed pore structure make them an interesting preform material for metal melt infiltration techniques. Thus, creep and wear resistant reinforcement structures of interpenetrating phase composites based on light weight metal (Al, Mg) composites is another intersting field of possible applications.

Acknowledgements

Financial support from Volkswagen-foundation under contract no. I/43073 is greatfully acknowledged.

References

1. Paris, O., Zizak, I., Lichtenegger, H., Roschger, P., Klaus Klaushofer, K. and Fratzl, P., Review: analysis of hierarchical structure of biological tissues by scanning X-ray scattering using a micro-beam. *Cell. Molec. Biology*, 2000, **46**, 993.
2. Jeronimidis, G., Structure-property relationships in biological materials. In *Structural Biological Materials. Pergamon Mat. Ser.*, ed. M. Elices. Pergamon, Amsterdam, 2000, p. 3.
3. Greil, P., Biomorphous ceramics from lignocellulosics. *J. Eur. Ceram. Soc.*, 2001, **21**, 105.
4. Byrne, C. E. and Nagle, D. C., Cellulose derived composites—a new method for materials processing. *Mater. Res. Innovat*. 1997, 137.
5. Byrne, C. E. and Nagle, D. C., Carbonization of wood for advanced materials applications. *Carbon*, 1997, **35**, 259.
6. Iizuka, H., Fushitani, M., Ohtsuka, M., Okabe, T., Saito, K. and Hokkirigawa, K., Mechanical properties of porous carbon materials i.e. woodcercamics. *J. Mat. Sci. Lett*., 1996, **15**, 1770.
7. Ota, T., Takahashi, M., Hibi, T., Ozawa, M. and Suzuki, H., Biomimetic process for producing SiC wood. *J. Am. Ceram. Soc*., 1995, **75**, 3409.
8. Greil, P., Lifka, T. and Kaindl, A., Biomorphic cellular silicon carbide ceramics from wood: I. Processing and microstructure. *J. Eur. Ceram. Soc*., 1998, **18,** 1961; Greil, P., Lifka, T. and Kaindl, A., Biomorphic cellular silicon carbide ceramics from wood. II. Mechanical properties. *J. Eur. Ceram. Soc*., 1998, **18**, 1975.
9. Shin, D. W. and Park, S. S., Silicon/silicon carbide composites fabricated by infiltration of a silicon melt into charcoal. *J. Am. Ceram. Soc*., 1999, **82**, 2251.
10. Singh, M., Environment conscious ceramics (ecoceramics). In *Proc. 24th Ann. Conf. on Composites, Advanced Ceramics, Materials, and Structurer: B, Cocoa Beach, FL 2000*, ed. T. Jessen and E. Ustundag. The Am. Ceram. Soc., Westerville, OH, 2000, pp. 39.
11. Vogli, E., Mukherji, J., Hofmann, Ch., Kladny, R., Sieber, H. and Greil, P., Conversion of oak to cellular silicon carbide ceramic by gas-phase reaction with silicon monoxide. *J. Am. Ceram. Soc*., 2001, **84**, 1236.
12. Gibson, L. J. and Ashby, M. F., *Cellular Solids, Structure and Properties*. Pergammon Press, New York, 1988.
13. Gibson, L. J., Wood: a natural fibre reinforced composite. *Metals and Materials*, 1992, **8**, 333.
14. Martinez-Fernandez, J., Valera-Feria, F. M. and Singh, M., High temperature compressive mechanical behavior of biomorphic silicon carbide ceramics. *Scripta Mater*., 2000, **43**, 813.
15. Kaindl, A., *Cellular SiC Ceramics from Wood*. PhD thesis, University of Erlangen-Nuernberg, Germany, 2000 (in German).
16. Sieber, H., Vogli, E., Müller, F., Greil, P., Popovska, N. and Gerhard, H., CVI-R gas phase processing of porous, biomorphic SiC-ceramics. *Key Engineering Materials*, 2001, **206–213**, 2013–2016.

17. Ritter, J. E., Jakus, J. K., Batakis, A. and Bandyopadhyay, N., Appraisal of biaxial strength testing. *J. Non-Cryst. Solids*, 1980, **38–39**, 419.
18. *MARC Reference Library*. MARC Anal. Res. Corp. Palo Alto, CA, 1997.
19. Paccaud, O., Derré, A., Silicon carbide coating by reactive pack cementation—part I: silicon carbide/silica interaction. *Chem. Vap. Deposition*, 2000, 6, 33; Paccaud, O., Derré, A., Silicon carbide coating by reactive pack cementation part—II: silicon monoxide/carbide reaction. *Chem. Vap. Deposition*, 2000, **6**, 41.
20. Jeronimidis, G., The fracture behaviour of wood and the relations between toughness and morphology. *Proc. Roy. Soc. Lond.*, 1980, **B208**, 447.
21. Kovar, D., King, B. H., Trice, R. W. and Halloran, J. W., Fibrous monolithic ceramics. *J. Am. Ceram. Soc.*, 1997, **80**, 2471.
22. Curtin, W. A., Fiber pullout and strain localization in ceramic-matrix composites. *J. Mech. Phys. Solids*, 1993, **41**, 35.
23. Clegg, W. J., Kendall, K., Alford, N.McN., Burton, T. W. and Birchall, J. D., A simple way to make tough ceramics. *Nature*, 1991, **347**, 455.
24. Phillips, A. J., Clegg, W. J., Clyne, T. W., Fracture behavior of ceramic laminates in bending: I. Modelling of crack-propagation and II. Comparison of model predictions with experimental data, *Acta Metall. Mater.*, 1993, **41**, 805; Phillips, A. J., Clegg, W. J., Clyne, T. W., Fracture behavior of ceramic laminates in bending: I. Modelling of crack-propagation. *Acta Metall. Mater.*, 1993, **41**, 819.